



Universidad Autónoma
de Madrid

Biblos-e Archivo
Repositorio Institucional UAM

Repositorio Institucional de la Universidad Autónoma de Madrid

<https://repositorio.uam.es>

Esta es la **versión de autor** del artículo publicado en:
This is an **author produced version** of a paper published in:

Journal of Chemical Physics 154.4 (2021): 044302

DOI: <https://doi.org/10.1063/5.0038047>

Copyright: © 2021 Author(s)

El acceso a la versión del editor puede requerir la suscripción del recurso
Access to the published version may require subscription

Significant bonding rearrangements triggered by Mg₄ clusters

Eva Vos,^[a] Inés Corral,^[a] M. Merced Montero-Campillo,^[a] Otilia Mó*^[a]

Departamento de Química (Módulo 13, Facultad de Ciencias) and Institute of Advanced Chemical Sciences (IadChem). Universidad Autónoma de Madrid. Campus de Excelencia UAM-CSIC. Cantoblanco, 28049-Madrid, Spain

Abstract

Among new nanostructures with exciting reactivity features, Mg₄ clusters present a promising catalytic behavior. The structure, stability and bonding of the complexes formed by the interaction of Mg₄ clusters and first row Lewis bases, namely ammonia, water and hydrogen fluoride, have been investigated through the use of high-level G4 single-reference and CASPT2 multireference formalisms. The adducts formed reflect the high electrophilicity of the Mg₄ cluster through holes in the neighborhood of each metallic center. After the adducts formation, the metallic bonding of the Mg₄ moiety is not significantly altered so the hydrogen shifts from the Lewis base toward the Mg atoms lead to new local minima with enhanced stability. For the particular case of ammonia and water, the global minima obtained when all the hydrogens of the Lewis base are shifted to the Mg₄ moiety have in common a very stable scaffold with a N or O center covalently tetracoordinated to the four Mg atoms, so the initial bonding arrangements of both reactants have completely disappeared.

Introduction

Nanoscience is probably one of the areas that has undergone the most spectacular development in the last two decades, as a direct result of the novel and unexpected properties exhibited by nanoparticles, with a typical size in the nm scale.^{1, 2} What makes nanoparticles so interesting is that their behavior and reactivity differ significantly from those of the bulk. In fact, the so called nano-effects are observed when reaching a critical size.³ Perhaps one of the most paradigmatic examples to illustrate the huge differences associated with the properties change in the size scale is gold, starting already with physical properties such as the melting point. Whereas the melting point of bulk gold is 1064° C, the melting point of gold nanoparticles of about 1.5 nm is less than half that value (500° C).⁴ Even the typical yellow color of this metal changes to blue for nanoparticles of around 50 nm or smaller.¹ The effects are also dramatic as far as the electron density distribution is concerned, as the nanoparticles do not have conduction bands and exhibit a rather peculiar reactivity. Indeed, whereas gold is usually considered an inert metal, gold nanoparticles are very reactive and behave as good catalysts.⁵⁻⁸ Rather importantly, this catalytic behavior seems to be closely related to the ability of gold nanoparticles to bind the reactants, this ability being also related to the size of the particle.^{8, 9} In general, it was also observed that within these nanoparticles, the low-coordinated gold atoms are more reactive, due to the presence of σ -holes associated with regions of depleted electron density,¹⁰ and therefore with positive electron potentials, which render them good electron acceptors. These findings corroborate that nanoparticles are well described by the same quantum chemistry formalisms commonly used to study molecules.

These features moved us to investigate the behavior of clusters involving alkaline-earth metals, because these elements, starting from Be and Mg, are characterized by being electron deficient elements. Indeed, this electron-deficiency is behind their rich chemistry through the formation of the so-called alkaline-earth (beryllium or magnesium) bonds.^{11, 12} The formation of alkaline-earth bonds results in a significant electron density redistribution of the Lewis base interacting with the Be or Mg derivative, modifying the Lewis base reactivity.^{13, 14} The consequence is that the formation of alkaline-earth bonds modulates the strength of other non-covalent interactions in which the Lewis base participates, such as hydrogen bonds,^{15, 16} halogen bonds,¹⁷⁻¹⁹ or tetrel bonds.^{20, 21} They also contribute to create σ -holes,²² or to spontaneously produce radicals.²³ In the same

direction, compounds that present beryllium containing groups physically close within the same molecular structure are shown to behave as extremely efficient electron²⁴ and anion sponges.^{25, 26}

In this study, we decided to focus our attention on Mg- rather than on Be-clusters, due to the high toxicity of Be. Previous theoretical studies on small Mg_n clusters found Mg_4 and Mg_{10} to be magic clusters, due to the completion of the valence shells with 8 and 20 electrons, respectively, in agreement with the predictions of the jellium model of metal clusters.²⁷ Later studies using molecular dynamics confirmed the magic nature of Mg_4 and Mg_{10} clusters.²⁸ Since our goal is to explore the interaction of small Mg clusters with conventional Lewis bases, namely ammonia, water and hydrogen fluoride, through the use of high level ab initio calculations, in the present study we will focus our attention on Mg_4 clusters. It is important to mention that it has been shown that bare Mg_n ($n < 80$) clusters can be efficiently obtained by the pickup of atoms into superfluid helium droplets.²⁹

Computational Details

It is well established that electron correlation effects are crucial to describe Mg_4 ,³⁰ whereas SCF calculations predict an almost unbound system.³¹ For the sake of high accuracy, we decided, initially, to use high-level G4 ab initio calculations to study the structure and stability of the complexes formed upon the interaction of Mg_4 clusters and the three Lewis bases indicated above. The G4 formalism is a composite method in which electron correlation effects are accounted for by using Moller-Plesset perturbation theory up to fourth-order and CCSD(T) coupled cluster theory, with a final correction for the Hartree-Fock limit evaluated using an extrapolation procedure and quadruple-zeta and quintuple-zeta basis sets.³² The standard G4 theory uses B3LYP/6-31G(2df,p) optimized geometries, but since in our case we are dealing with weak interactions, where dispersion effects may be important as well as the use of diffuse functions, we decided to use a MP2/aug-cc-pVTZ formalism, instead of the standard B3LYP/6-31G(2f,p) one, to obtain the geometries and the thermochemical corrections in our G4-type calculations. In fact, correlation effects were found to be crucial already to describe the bonding between Lewis bases and single Mg atom, showing a considerable charge polarization of the electron density on the metal.³³

Since, as mentioned above, the description of Mg_n and Be_n clusters, represent a challenge from the theoretical viewpoint, due to the crucial role of electron correlation effects,^{30, 34} we have also explored whether a single reference formalism would be appropriate. Quite unexpectedly, we found that single-reference procedures present for Mg_4 and $\text{Mg}_4\text{-LB}$ (LB = Lewis base) complexes an RHF-UHF instability, to the best of our knowledge, not reported before in the literature. Therefore, we have resorted to a multireference approach to describe these systems. In particular, all the $\text{Mg}_4\text{-LB}$ clusters were optimized with the SS-CASPT2^{35, 36} method combined with the cc-pVTZ basis set,^{37, 38} as implemented in Bagel software.³⁹ Different active spaces, including from 8 up to 12 orbitals, were employed for the construction of the CASSCF reference wavefunctions, depending on the Lewis base considered. The active spaces of the three families of adducts include 8 out of the 12 orbitals built from the linear combination of the 3p orbitals of the Mg atoms (the most correlated occupied and unoccupied orbitals). Additionally, the active spaces for $\text{Mg}_4\text{-H}_2\text{O}$ and $\text{Mg}_4\text{-HF}$ complexes respectively include 2 and 1 pair of σ and σ^* orbitals sitting on the Lewis base. Final energies, in the case of the $\text{Mg}_4\text{-NH}_3$ clusters, were recomputed augmenting the active space in 6 extra orbitals, corresponding to the σ and σ^* orbitals of NH_3 . The active space composition for the initial **a1**, **w1** and **hfl** adducts are collected in figures S1-S8 of the Supplementary Material. To reduce the computational cost of these calculations we have excluded the 1s orbitals of all the heavy atoms from the correlation treatment and we have employed the density fitting approach. The required auxiliary basis set for the density fitting calculation was generated using the PySCF code.⁴⁰

The multireference character of the localized minima was quantitatively evaluated with the multireference diagnostic, M , from Truhlar and coworkers, defined in this particular case, (closed shell systems), in terms of the natural orbital occupation numbers of the most correlated occupied and unoccupied natural orbitals.⁴¹

To analyze the bonding characteristics of the complexes under investigation, we have initially used the molecular electrostatic potential (MEP) which corresponds to the (attractive or repulsive) potential that a unit positive charge experiences when approaching the cluster. This potential defined as:

$$V(\mathbf{r}) = \sum_A \frac{Z_A}{|\mathbf{R}_A - \mathbf{r}|} - \int \frac{\rho(\mathbf{r}') d\mathbf{r}'}{|\mathbf{r}' - \mathbf{r}|}$$

where Z_A and \mathbf{R}_A are the charge and position of nucleus A, and $\rho(\mathbf{r})$ is the electron density, and usually provides reliable information on the electrophilicity or nucleophilicity of a given site of the system. The MEP is also a good procedure to detect the existence of σ -holes. A second useful approach is the quantum theory of atoms in molecules (QTAIM),^{42, 43} able to locate the critical points of the electron density of any chemical system. The values of the electron density at the so-called bond critical points (BCPs) are a good measure of the strength of the linkage and provide also information about its covalent character, through the values and sign of the Laplacian and the energy density. This information is nicely complemented by the one obtained by using other two alternative formalisms, namely the Non-covalent Interaction (NCI) index formalism.^{44, 45} and the electron localization function (ELF).⁴⁶ The NCI is a method based on the use of the reduced density gradient that allows to find regions in the real space where these interactions do actually take place, distinguishing qualitatively and quantitatively between strong or weak attractive and repulsive interactions. The ELF function divides the molecular space in different kinds of basins that can be associated with core electrons, lone pairs (monosynaptic), and bonding regions (disynaptic or polysynaptic basins). A more detailed description of these three procedures has been included in the Supplementary Material.

Results and Discussion

Mg₄ cluster

As previously reported in the literature,^{27, 28, 30, 47} our MP2/aug-cc-pVTZ geometry optimizations indicate that Mg₄ clusters exhibit a tetrahedral structure, with Mg-Mg bond distances of 3.047 Å. The G4 calculated binding energy on this structure is 38.6 kJ/mol per atom, which is significantly lower than the value obtained using density-functional molecular dynamic methods (51.1 kJ/mol per atom),²⁷ but in rather good agreement -only slightly higher- than previous Born-Oppenheimer local-spin-density molecular dynamics reported values (34.7 and 38.6 kJ/mol per atom).²⁸

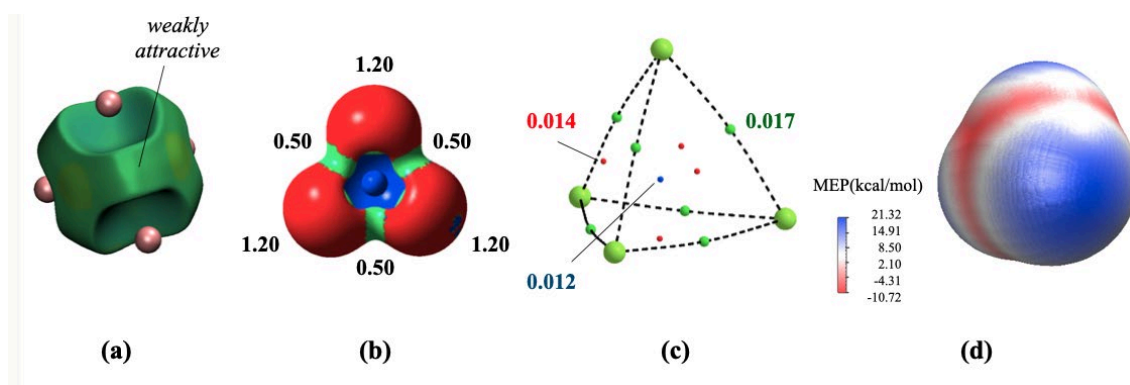


Figure 1. Bonding characteristics for Mg_4 . a) NCI 3D plot; b) ELF(= 0.75) plot; c) AIM molecular graph; d) molecular electrostatic potential on the 0.001 au isodensity surface. . In the ELF plots, the numbers correspond to the electron populations of the different monosynaptic (red lobes) or trisynaptic basins (green lobes). In the AIM molecular graph, the green, red and blue dots indicate bond, ring and cage critical points, respectively. The electron densities at these points are in au. In the MEP, blue areas indicate the most positive sites, i.e., electrophilic areas for preferential nucleophilic attack.

As far as the bonding features are concerned, the NCI 3D plot in Fig. 1a shows that the Mg_4 tetrahedral cluster exhibits a structure in which the four Mg atoms share their valence electron pairs leading to a typical metallic bonding arrangement. Consistently, the corresponding NCI 2D plot in the attractive region (see Fig. S9 in the Supplementary Material) presents a single peak at low density values. This metallic character is also seen in the ELF plot (Fig. 1b) showing different trisynaptic basins (green) at the edges of the tetrahedron whereas the population at the corners is located in monosynaptic (red) basins. The molecular graph obtained with the AIM method also corroborates this metallic character because the electron densities at the bond, ring and cage critical points are very close, indicating a rather complete electron delocalization. Very interestingly however, the molecular electrostatic potential of Mg_4 (see Figure 1d) shows at the corners of the tetrahedron well defined areas of positive potential (holes), associated with preferential sites for nucleophilic interactions. Similar situations have been reported for other metallic clusters like gold,¹⁰ but likely due to the electron-deficient character of Mg, the values reported here for these Mg_4 positive potentials are more than twice larger.

Mg₄-L (L = NH₃, H₂O, HF) complexes

As expected from the characteristics of the molecular electrostatic potential around the Mg₄ cluster described in the previous section, its interaction with the Lewis bases included in our study implies the nucleophilic attack of the base on one of the electrophilic Mg atoms. This is illustrated in Figure 2 for the particular case of ammonia, but similar results are obtained when dealing with water or hydrogen fluoride as illustrated in Fig. S10 of the Supplementary Material.

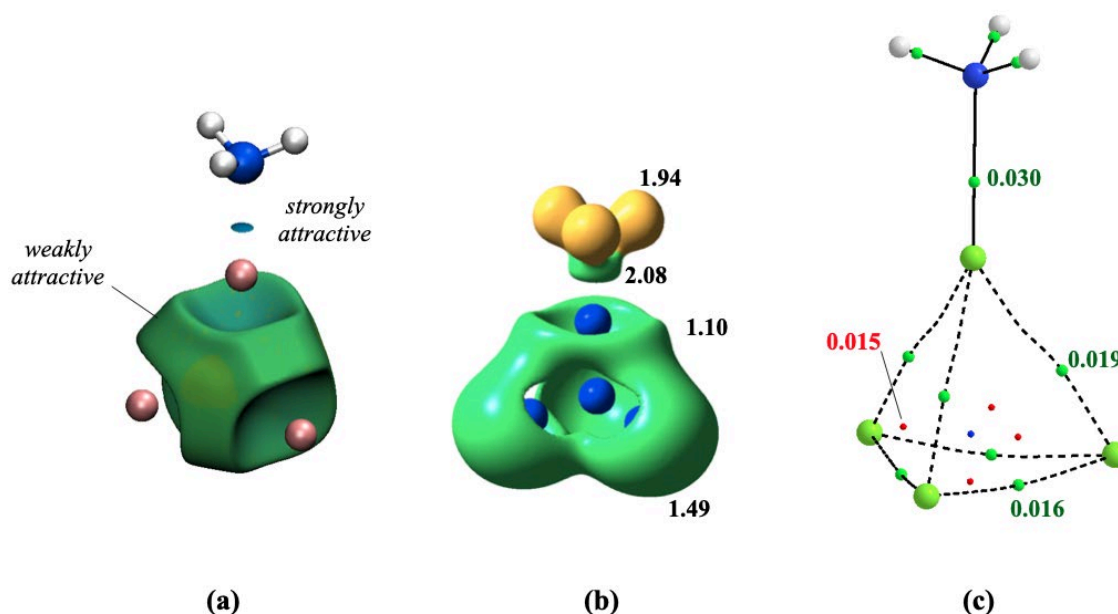


Figure 2. Bonding characteristics for Mg₄-NH₃ adduct showing the NCI 3D (a), the ELF(= 0.75) plot (b) and the AIM molecular graph (c). Same conventions as in Figure 1.

A comparison of the NCI 3D in Figures 1a and 2a shows that the interaction with ammonia does not perturb significantly the metallic bond observed for the isolated Mg₄ cluster. A new and stronger interaction (blue disc) appears between N and Mg. Something similar is observed when looking at the ELF representation (Fig. 2b) though a new disynaptic basin between one of the Mg atoms and the N of ammonia appears, as a consequence of the nucleophilic-electrophilic interaction between the N-lone pair and the hole at the Mg atom. It can be also observed that this interaction slightly enhances the volume and population around the Mg atoms, so all basins are now polysynaptic (green). Consistently, the molecular graph (Fig. 2c) shows the formation of a new Mg-N bond, but the remaining Mg-Mg bonds in the Mg₄ moiety are not very much altered with respect to those in the isolated cluster (recall Fig. 1c).

As it could be expected from the nature of the $\text{Mg}_4\text{-LB}$ ($\text{LB}=\text{NH}_3$, H_2O , HF) interaction, the binding energy (BE), defined as the energy needed to dissociate each complex into the two non-interacting systems, decreases remarkably for the corresponding adducts **a1**, **w1**, and **hf1** (see Fig. 3) from the best electron donor of the three bases, ammonia (61 kJ/mol), to the poorest electron donor, hydrogen fluoride (19 kJ/mol).

However, the fact that the electron density distribution around the Mg_4 moiety is not substantially altered in the adduct permits to guess that most of its bonding capacity is still almost intact. To investigate whether this is indeed the case, we have explored the existence and stability of new isomers that could be obtained by hydrogen shifts from the Lewis base towards the Mg_4 moiety. The most stable minima found after successive hydrogen shifts are also shown in Fig. 3 (**a2-a6**, **w2-w5**, **hf2-hf3**). Other less stable conformations than those shown in this figure are presented in Fig. S11 of the Supplementary Material.

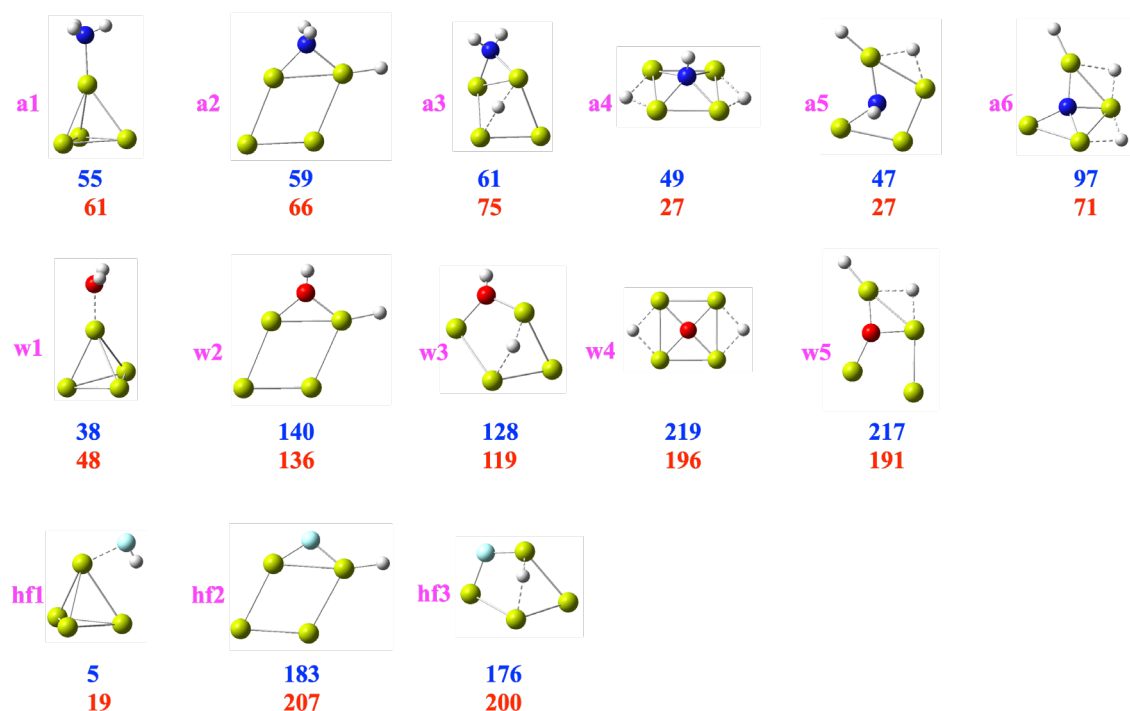


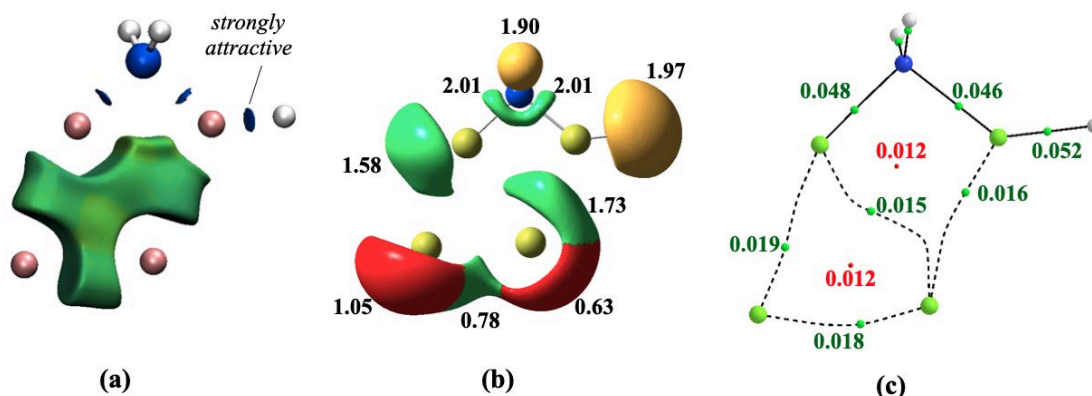
Figure 3. G4 (blue) and CASPT2 (red) binding energies ($\text{kJ}\cdot\text{mol}^{-1}$) of different conformers for the complexes between Mg_4 and ammonia, water and hydrogen fluoride. The adducts are shown in the first column. The isomers formed from the adducts after (i) a single hydrogen shift, (ii) a double hydrogen shift and (iii) after three hydrogen shifts are shown in the second and third columns, in the fourth and fifth columns, and in the sixth column, respectively.

In Fig. 3, we are reporting both the high-level single-reference and multireference BEs. It can be seen that both sets of values are similar, but more importantly there are linearly correlated, as shown in Fig. S12 of the Supplementary Material. However, taking into account that single-reference wave functions are affected, as mentioned above, by RHF/UHF instabilities, for the discussion that follows, we will use the multi-reference values. This is supported by the analysis of the CASSCF wave functions of all the species investigated here which, except for the Lewis bases, NH_3 , H_2O and HF , show from moderate ($0.05 < M < 0.1$: Mg_4 , **a1**, **w1**, **hf1**) to strong multireference character ($M > 0.1$ rest of the minima), see Tables S1-S4 in the Supplementary Material. The values of the multireference diagnostic are consistent with the weight of the close shell configuration which is for all the calculated complexes below 0.85, with the second most important configuration corresponding to excitation among 3p orbitals sitting on the Mg_4 moiety. Remarkably, the largest multiconfigurational character is found for the minima either showing three center H-Mg-H bonds or with a H bridging between two non-directly bonded Mg atoms.

Looking at the values in Figure 3, it is very interesting to note that, whereas the stability of the adducts (**a1**, **w1**, **hf1**), follows, as previously mentioned, the trend $\text{NH}_3 > \text{H}_2\text{O} > \text{HF}$, the stability of the most stable minima associated to a single hydrogen shift (**a2**, **w2**, **hf2**) follows the opposite trend, $\text{NH}_3 < \text{H}_2\text{O} < \text{HF}$.

This can be understood by looking in detail to the bonding changes induced by the hydrogen shift. Let us take the complex with ammonia as a suitable example to do this analysis. In the process of going from the $\text{Mg}_4\text{-NH}_3$ adduct **a1** to the MgH-NH_2 complex **a2**, one of the N-H bonds is replaced by a Mg-H bond, leaving the N atom with capacity to bind to a second Mg atom. Indeed, in the new **a2** structure, once the new covalent Mg-H bond has been formed, the nitrogen atom of the remaining NH_2 group is able to covalently bind two Mg atoms. Moreover, the ELF of this complex shows the existence of a disynaptic Mg-H basin (yellow lobe in Fig. 4b), and two disynaptic N-Mg basins (green lobes) each of them occupied by an electron pair. Consistently, the molecular graph of the **a2** complex (Fig. 4c) shows that the electron densities at the Mg-N BCPs are 53% higher (0.046 and 0.048 au) than the value in the **a1** adduct (0.030 au, Fig. 2c). Also coherently, both Mg-N bonds in **a2** are 0.16 Å shorter than the Mg-N bond in **a1**. In summary, the hydrogen shift going from Mg_4NH_3 to the most stable MgH-NH_2 complex not only increases the number of Mg-N bonds, but also the strength of these

linkages. It should be mentioned that similar bridged structures were reported in a previous study of $(\text{MgF}_2)_n$ ($n=2-3$) by Francisco et al.⁴⁸



The changes observed for the complexes with water and hydrogen fluoride are qualitatively similar, but quantitatively stronger. Indeed, as illustrated in Fig. S13 of the Supplementary Material, the increase in the electron density of the Mg-O and Mg-F bonds on going from the adducts **w1** and **hf1** to the new isomers **w2** and **hf2** (Fig. 3) is greater (85% and 91%) than that calculated for the N-containing analogue. This is again reflected in the larger shortening undergone by the Mg-O and Mg-F bonds (0.20 Å for the former, and 0.24 Å for the latter) than the one found for the Mg-N bonds. The conformers **a3**, **w3**, **hf3** only differ in the position of the shifted hydrogen, now bridging between two Mg atoms, and their relative stabilities are not much different from the isomers **a2**, **w2**, **hf2**.

The behavior of the nitrogen containing complexes upon a second hydrogen shift differ significantly from that of the oxygen-containing ones. Whereas for the latter, a second hydrogen shift to yield the structure **w4** implies a significant stabilization of the system (ca. 80 kJ·mol⁻¹), this is not the case for the analogous structure **a4**, where the process involves a decrease (ca. 20 kJ·mol⁻¹) on the stability of the complex. These two complexes actually differ in their symmetry, as complex **a4** belongs to the C_{2v} symmetry point group, whereas the **w4** complex is a D_{2h} structure. In fact, the N and O basic sites appear in both cases bonded to the four Mg atoms. However, whereas the O atom lies in the same plane as the four Mg atoms, the N atom does not. As N is less electronegative,

its volume is larger and cannot be accommodated at the center of the square defined by the four Mg atoms. These differences are evident when looking at the different ELF basins volumes around N and O (Fig. 5), which show that both nitrogen and oxygen in **a4** and **w4** present a ring-polysynaptic basin with a population (~ 7.86 e) of practically four pairs. In addition, the N atom in **a4** is pentacoordinated through a covalent bond to one H atom, but in this case the basic site is 0.78 Å above the center of the ring. The obvious consequence is that the bonding is necessarily much weaker. This description is corroborated by the fact that a third hydrogen shift connecting **a4** with **a6** leads to a significant stabilization of the system (ca. $70 \text{ kJ}\cdot\text{mol}^{-1}$). As shown by the **a6** ELF plot in Fig. 5, the attachment of the third hydrogen atom to one of the Mg bonds breaks the symmetry of the system. Although N is still tetracoordinated to four Mg atoms, this time they lie on the same plane, rendering the system much more stable.

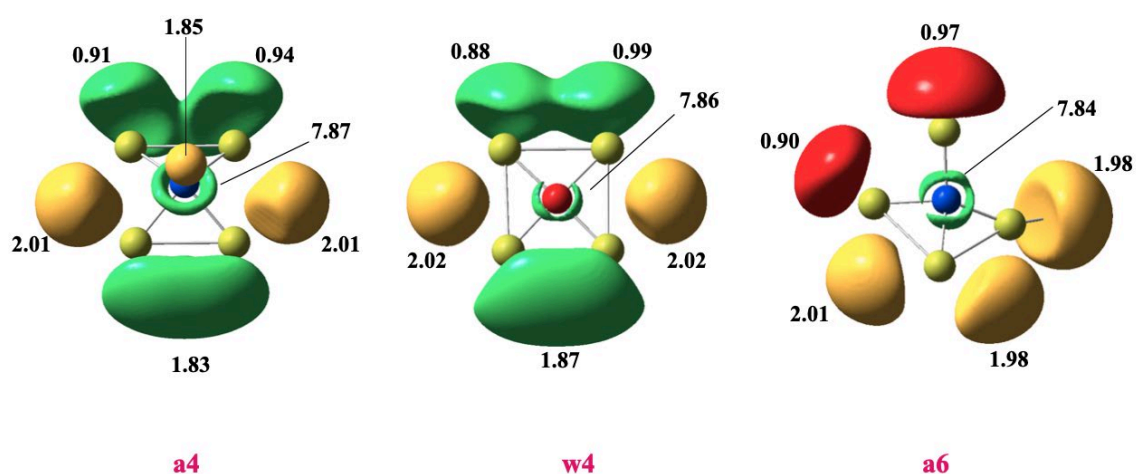


Figure 5. ELF($= 0.85$) plots for complexes **a4**, **w4** and **a6**. Same conventions as in Figure 1.

Concluding remarks

The interaction of Mg_4 clusters with conventional Lewis bases yields stable complexes reflecting the electrophilicity of the former, which as other metal clusters presents electro-deficient regions revealed by the MEP in the neighborhood of the metallic centers. The formation of these adducts does not significantly alter the metallic bonding of the Mg_4 cluster, so that successive hydrogen-shift processes from the Lewis base towards the Mg_4 moiety results in the formation of new very stable isomers in which from two to four Mg atoms are covalently bonded to the basic site (N, O, F) of the Lewis

base. The global minima are those for which the basic site has the largest possible coordination number with the Mg atoms and exhibit binding energies of hundreds of kJ/mol at the CASPT2 level. In other words, the initial bonding arrangement of both the Mg₄ cluster and the Lewis base has completely disappeared in the most stable structures, and their stability is closely related to hypervalent N, O and F atoms.

Dedication

This paper is dedicated to all the mothers who fight for a better education of their children

Acknowledgements

This work is supported by the projects PGC2018-094644-B-C21, PGC2018-094644-B-C22 and PID2019-110091GB-I00 (MICINN) of the Ministerio de Ciencia, Innovación y Universidades of Spain, the Ramón y Cajal program and a Formación de Profesorado Universitario (FPU) contract from the Ministerio de Economía, Industria y Competitividad of Spain. We are grateful to Profs. Elguero, Alkorta and Yáñez for helpful comments. Thanks are also given to the CTI (CSIC), the CESGA Supercomputing Center and the Centro de Computación Científica of the UAM (CCC-UAM) for their computational support.

Data Availability

Data available in article or Supplementary Material

References

1. G. E. Schmid, *Nanoparticles. From theory to application*. (Wiley-VCH, Weinheim, 2004).
2. G. A. Ozin, A. C. Arsenault and L. Cademariti, *Nanochemistry. A chemical approach to nanomaterials*. (The Royal Society of Chemistry London, 2009).
3. G. B. Sergeev and K. J. Kalbunde, *Nanochemistry (2nd. Edition)*. (ScienceDirect. Elsevier B.V., Amsterdam, 2013).
4. T. Castro, R. Reifengerger, E. Choi and R. P. Andres, *Phys. Rev. B* **42** (13), 8548-8556 (1990).
5. G. C. Bond and D. T. Thompson, *Catal. Rev.-Sci. Eng.* **41** (3-4), 319-388 (1999).
6. B. Hvolbaek, T. V. W. Janssens, B. S. Clausen, H. Falsig, C. H. Christensen and J. K. Nørskov, *Nano Today* **2** (4), 14-18 (2007).
7. M. Stratakis and H. Garcia, *Chem. Rev.* **112** (8), 4469-4506 (2012).
8. S. W. Cao, F. Tao, Y. Tang, Y. T. Li and J. G. Yu, *Chem. Soc. Rev.* **45** (17), 4747-4765 (2016).

9. C. Lemire, R. Meyer, S. Shaikhutdinov and H. J. Freund, *Angew. Chem. Int. Ed.* **43** (1), 118-121 (2004).
10. J. H. Stenlid and T. Brinck, *J. Am. Chem. Soc.* **139** (32), 11012-11015 (2017).
11. M. Yáñez, P. Sanz, O. Mó, I. Alkorta and J. Elguero, *J. Chem. Theor. Comput.* **5**, 2763-2771 (2009).
12. R. Tama, O. Mo, M. Yanez and M. M. Montero-Campillo, *Theor. Chem. Acc.* **136** (3), 9 (2017).
13. M. M. Montero-Campillo, O. Brea, O. Mó, I. Alkorta, J. Elguero and M. Yáñez, *Phys. Chem. Chem. Phys.* **21** (5), 2222-2233 (2019).
14. O. Mó, M. M. Montero-Campillo, I. Alkorta, J. Elguero and M. Yez, *Chem.-Eur. J.* **25** (50), 11688-11695 (2019).
15. O. Mó, M. Yáñez, I. Alkorta and J. Elguero, *J. Chem. Theory Comput.* **8**, 2293-2300 (2012).
16. L. Albrecht, R. J. Boyd, O. Mó and M. Yáñez, *Phys. Chem. Chem. Phys.* **14** (42), 14540-14547 (2012).
17. I. Alkorta, J. Elguero, O. Mó, M. Yáñez and J. E. Del Bene, *Phys. Chem. Chem. Phys.* **17** (3), 2259-2267 (2015).
18. V. Oliveira, E. Kraka and D. Cremer, *Phys. Chem. Chem. Phys.* **18** (48), 33031-33046 (2016).
19. Y. Tao, Y. Qiu, W. Zou, S. Nanayakkara, S. Yannacone and E. Kraka, *Molecules* **25** (7) (2020).
20. I. Alkorta, M. M. Montero-Campillo, O. Mó, J. Elguero and M. Yáñez, *J. Phys. Chem. A* **123**, 7124-7132 (2019).
21. D. Sethio, V. Oliveira and E. Kraka, *Molecules* **23** (11), 21 (2018).
22. O. Brea, O. Mó, M. Yáñez, I. Alkorta and J. Elguero, *Chem. Eur. J* **21** (36), 12676-12682 (2015).
23. O. Brea, I. Alkorta, O. Mó, M. Yáñez, J. Elguero and I. Corral, *Angew. Chem. Eng. Int. Ed.* **55**, 8736-8739 (2016).
24. O. Brea, O. Mó, M. Yáñez, I. Alkorta and J. Elguero, *Chem. Commun.* **52**, 9656-9659 (2016).
25. O. Brea, I. Corral, O. Mó, M. Yáñez, I. Alkorta and J. Elguero, *Chem. Eur. J.* **22**, 18322-18325 (2016).
26. M. M. Montero-Campillo, O. Mo, M. Yanez, I. Alkorta and J. Elguero, *Chemphyschem* **19** (14), 1701-1706 (2018).
27. V. Kumar and R. Car, *Phys. Rev. B* **44** (15), 8243-8255 (1991).
28. J. Akola, K. Rytönen and M. Manninen, *Eur. Phys. J. D* **16** (1-3), 21-24 (2001).
29. T. Diederich, T. Doppner, J. Braune, J. Tiggesbaumker and K. H. Meiwes-Broer, *Phys. Rev. Lett.* **86** (21), 4807-4810 (2001).
30. R. A. Chiles, C. E. Dykstra and K. D. Jordan, *J. Chem. Phys.* **75** (2), 1044-1046 (1981).
31. K. D. Jordan and J. Simons, *J. Chem. Phys.* **72** (4), 2889-2890 (1980).
32. L. A. Curtiss, P. C. Redfern and K. Raghavachari, *J. Chem. Phys.* **126** (8), 84108 (2007).
33. L. A. Curtiss, E. Kraka, J. Gauss and D. Cremer, *J. Phys. Chem.* **91** (5), 1080-1084 (1987).
34. M. M. Montero-Campillo, O. Mó, M. Yáñez, I. Alkorta and J. Elguero, in *Computational Chemistry*, edited by R. VanEldik and R. Puchta (Elsevier Academic Press Inc, San Diego, 2019), Vol. 73, pp. 73-121.
35. K. Andersson, P. A. Malmqvist, B. O. Roos, A. J. Sadlej and K. Wolinski, *J. Phys. Chem.* **94** (14), 5483-5488 (1990).

36. K. Andersson, P. A. Malmqvist and B. O. Roos, *J. Chem. Phys.* **96** (2), 1218-1226 (1992).
37. T. H. Dunning, *J. Chem. Phys.* **90** (2), 1007-1023 (1989).
38. B. P. Prascher, D. E. Woon, K. A. Peterson, T. H. Dunning and A. K. Wilson, *Theor. Chem. Acc.* **128** (1), 69-82 (2011).
39. BAGEL, Brilliantly Advanced General Electronic-structure Library. <http://www.nubakery.org> under the GNU General Public License.
40. Q. M. Sun, T. C. Berkelbach, N. S. Blunt, G. H. Booth, S. Guo, Z. D. Li, J. Z. Liu, J. D. McClain, E. R. Sayfutyarova, S. Sharma, S. Wouters and G. K. L. Chan, *Wiley Interdiscip. Rev.-Comput. Mol. Sci.* **8** (1), 15 (2018).
41. O. Tishchenko, J. J. Zheng and D. G. Truhlar, *J. Chem. Theory Comput.* **4** (8), 1208-1219 (2008).
42. R. F. W. Bader, *Atoms in Molecules. A Quantum Theory*. (Clarendon Press, Oxford, 1990).
43. P. L. A. Popelier, in *Intermolecular Forces and Clusters I. Structure and Bonding*, edited by D. J. Wales (Springer, Berlin, Heidelberg, 2005), Vol. 115.
44. J. Contreras-García, E. R. Johnson, S. Keinan, R. Chaudret, J. P. Piquemal, D. N. Beratan and W. T. Yang, *J. Chem. Theory Comput.* **7** (3), 625-632 (2011).
45. R. A. Boto, F. Peccati, R. Laplaza, C. Quan, A. Carbone, J.-P. Piquemal, Y. Maday and J. Contreras-García, *J. Chem. Theory Comp.* **16**, 4150-4158 (2020).
46. A. Savin, R. Nesper, S. Wengert and T. F. Fassler, *Angew. Chem.-Int. Edit.* **36** (17), 1809-1832 (1997).
47. G. Pacchioni and J. Koutecky, *J. Chem. Phys.* **77** (11), 5850-5851 (1982).
48. E. Francisco, A. Martín-Pendás and A. Costales, *J. Phys. Chem. A* **106** (2), 335-344 (2002).

Significant bonding rearrangements triggered by Mg₄ clusters

Eva Vos, Inés Corral, M. Merced Montero-Campillo, Otilia Mó

Contribution from the Departamento de Química (Módulo 13, Facultad de Ciencias) and Institute of Advanced Chemical Sciences (IadChem). Universidad Autónoma de Madrid. Campus de Excelencia UAM-CSIC. Cantoblanco, 28049-Madrid, Spain

Supplementary Material

(A total of 13 Pages)

Contents

Pages 16-17. M diagnostic for the Mg_4 -clusters, Mg_4 and the Lewis bases (Table S1-S4)

Page 17-21. Selected active space for the Mg_4 -cluster, Mg_4 and the Lewis bases (Figs. S1-S8)

Page 22. NCI-2D plots for the isolated Mg_4 cluster and a set of selected Mg_4-NH_3 clusters a1, a4 and a6 (Fig. S9)

Page 23. Bonding analysis for Mg_4-H_2O and Mg_4-HF adducts including NCI 3D, ELF and AIM molecular graphs (Fig. S10)

Page 24. Additional local minima arising from the interaction of Mg_4 with NH_3 , H_2O and HF (Fig. S11), and Linear correlation between the CASPT2 and G4 calculated binding energies for complexes of Mg_4 (Fig. S12)

Page 25. Molecular graphs for the adducts between water or hydrogen fluoride with Mg_4 clusters and the most stable local minima (Fig. S13).

Page 26-27. Additional Computational Details.

Table S1: Weight of the Hartree-Fock and the second most contributing configurations to the CASSCF(6,8)/cc-pVTZ wave function and M values for the Mg_4-NH_3 minima. (CASSCF(12,14)/cc-pVTZ values within parenthesis).

Structure	M value	Hartree Fock and second configuration weight
a1	0.093 (0.092)	0.848/0.009 (0.824/0.008)
a2	0.138 (0.159)	0.860/0.018 (0.790/0.033)
a3	0.204 (0.208)	0.836/0.082 (0.761/0.056)
a4	0.221 (0.244)	0.858/0.097 (0.760/0.090)
a5	0.192 (0.238)	0.866/0.082 (0.776/0.079)
a6	0.343 (0.327)	0.798/0.161 (0.764/0.144)

Table S2: Weight of the Hartree-Fock and the second most contributing configurations to the CASSCF(10,12)/cc-pVTZ wave function and M values for Mg₄-H₂O minima.

Structure	M value	Hartree Fock and second configuration weight
w1	0.092	0.835/0.009
w2	0.126	0.849/0.022
w3	0.219	0.794/0.086
w4	0.207	0.845/0.089
w5	0.168	0.865/0.079

Table S3: Weight of the Hartree-Fock and the second most contributing configurations to the CASSCF(8,10)/cc-pVTZ wave function and M values for the Be₂-HF minima.

Structure	M value	Hartree Fock and second configuration weight
hf1	0.089	0.848/0.008
hf2	0.162	0.810/0.037
hf3	0.221	0.767/0.067

Table S4: Weight of the Hartree-Fock and the second most contributing configurations to the CASSCF/cc-pVTZ wave function and M values for Mg₄, HF, H₂O and NH₃. The size of the active spaces is indicated within parenthesis.

Structure	M value	Hartree Fock configuration weight
Mg ₄ (6,8)	0.077	0.867
NH ₃ (6,6)	0.022	0.969
H ₂ O(6,6)	0.023	0.969
HF(6,6)	0.022	0.975

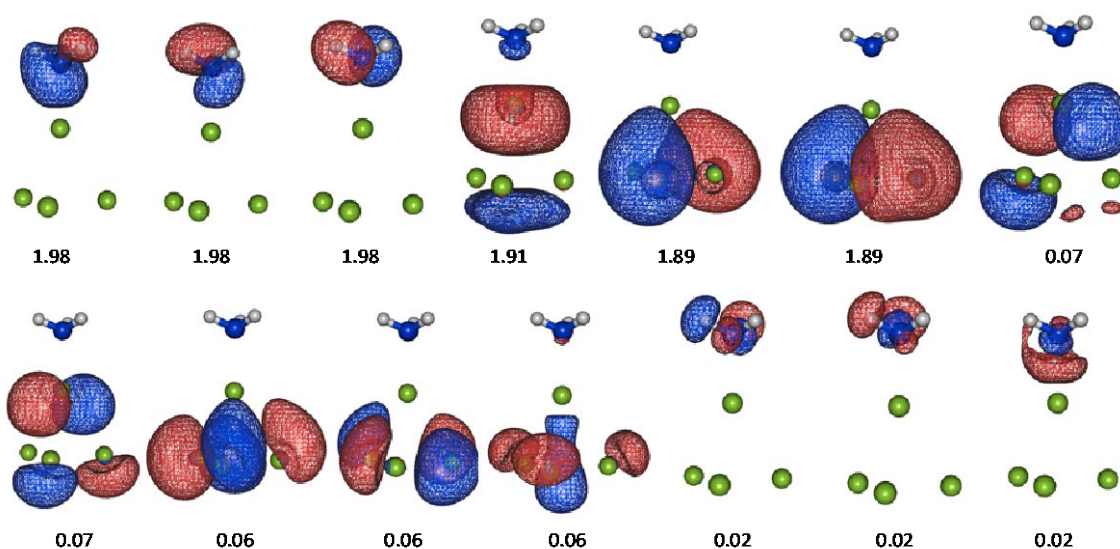


Figure S1. CASSCF orbitals with their occupation numbers included in the (12,14) active space of $\text{Mg}_4\text{-NH}_3$ at the **a1** structure.

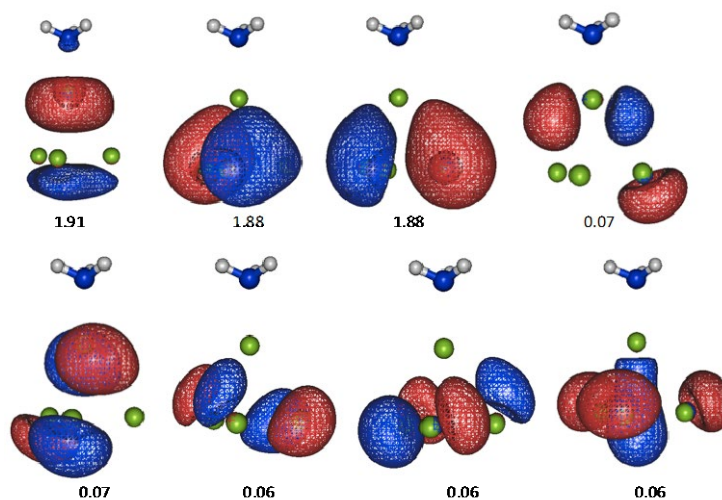


Figure S2. CASSCF orbitals with their occupation numbers included in the reduced (6,8) active space of $\text{Mg}_4\text{-NH}_3$ at the **a1** structure.

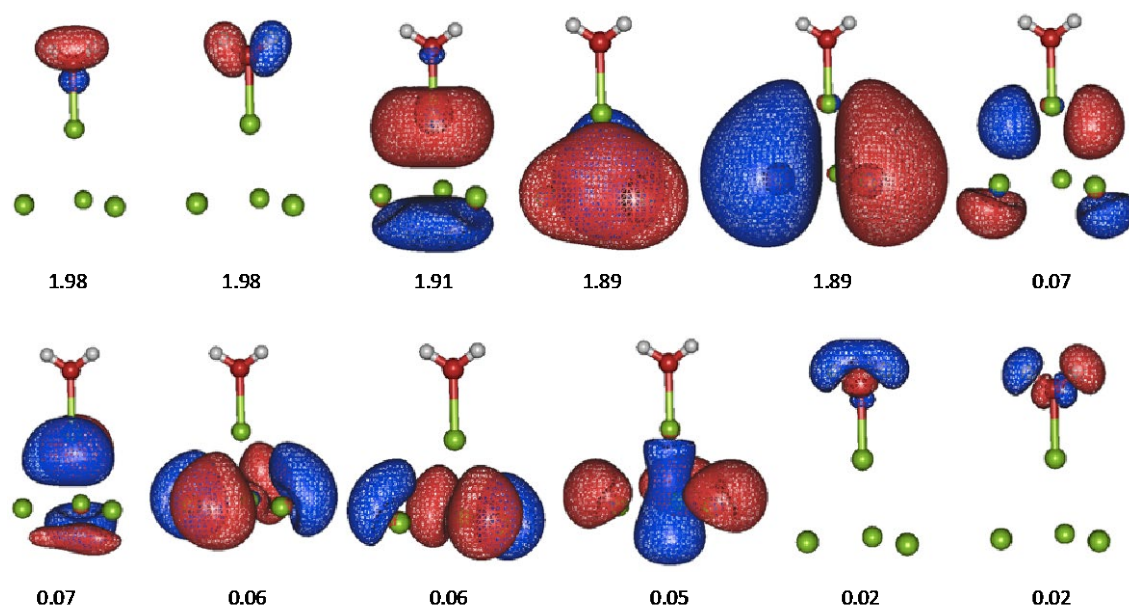


Figure S3. CASSCF orbitals with their occupation numbers included in the (10,12) active space of $\text{Mg}_4\text{-H}_2\text{O}$ at the **w1** structure.

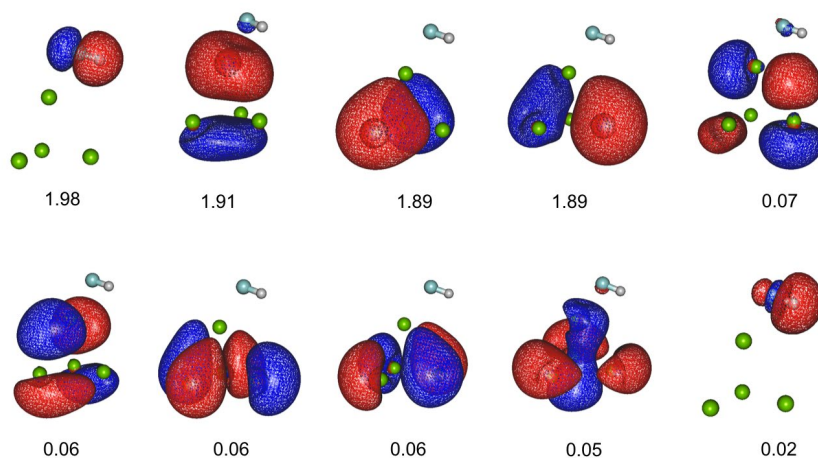


Figure S4. CASSCF orbitals with their occupation numbers included in the (8,10) active space of $\text{Mg}_4\text{-HF}$ at the **hfl** structure.

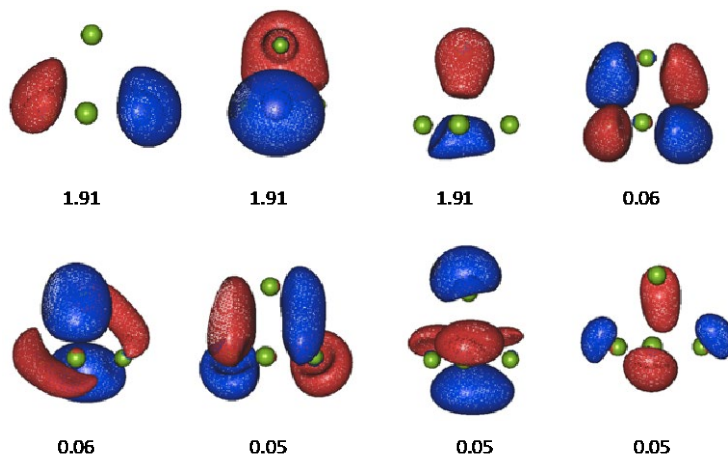


Figure S5. CASSCF orbitals with their occupation numbers included in the (6,8) active space of the isolated Mg_4 cluster.

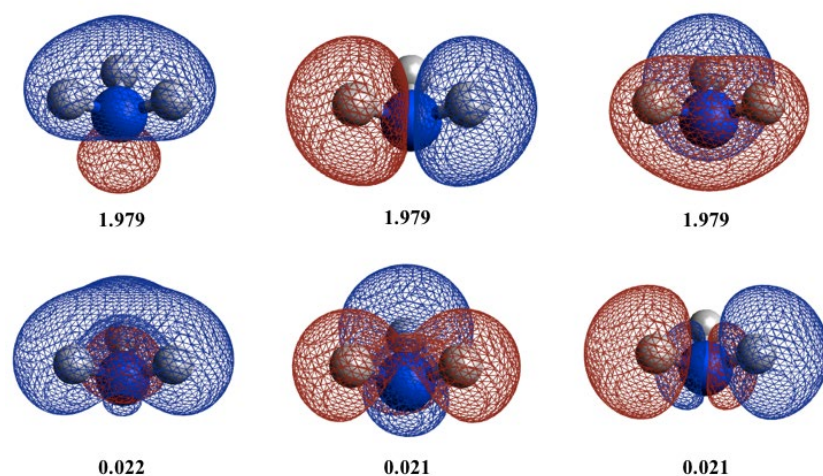


Figure S6. CASSCF orbitals with their occupation numbers included in the (6,6) active space of the isolated NH_3 molecule.

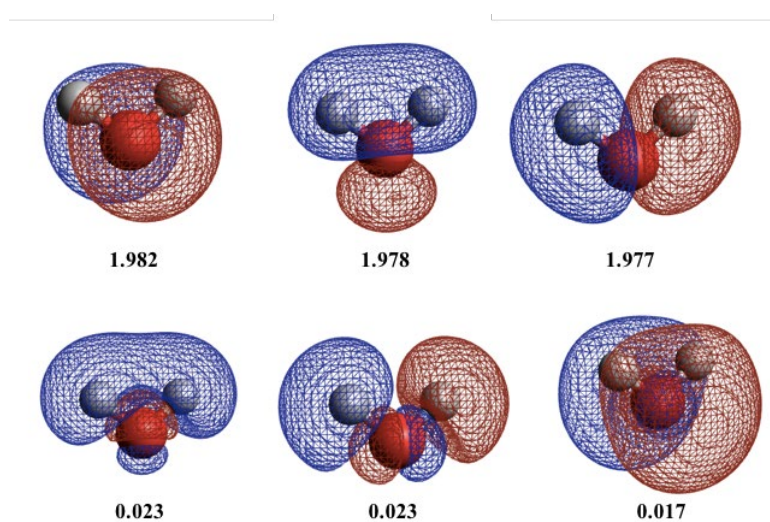


Figure S7. CASSCF orbitals with their occupation numbers included in the (6,6) active space of the isolated H_2O molecule.

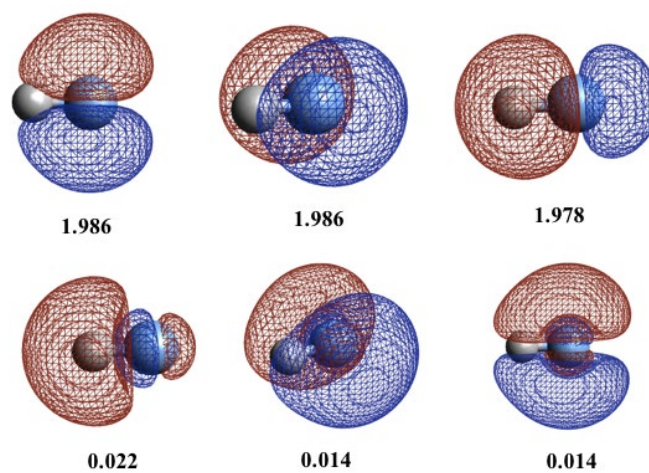
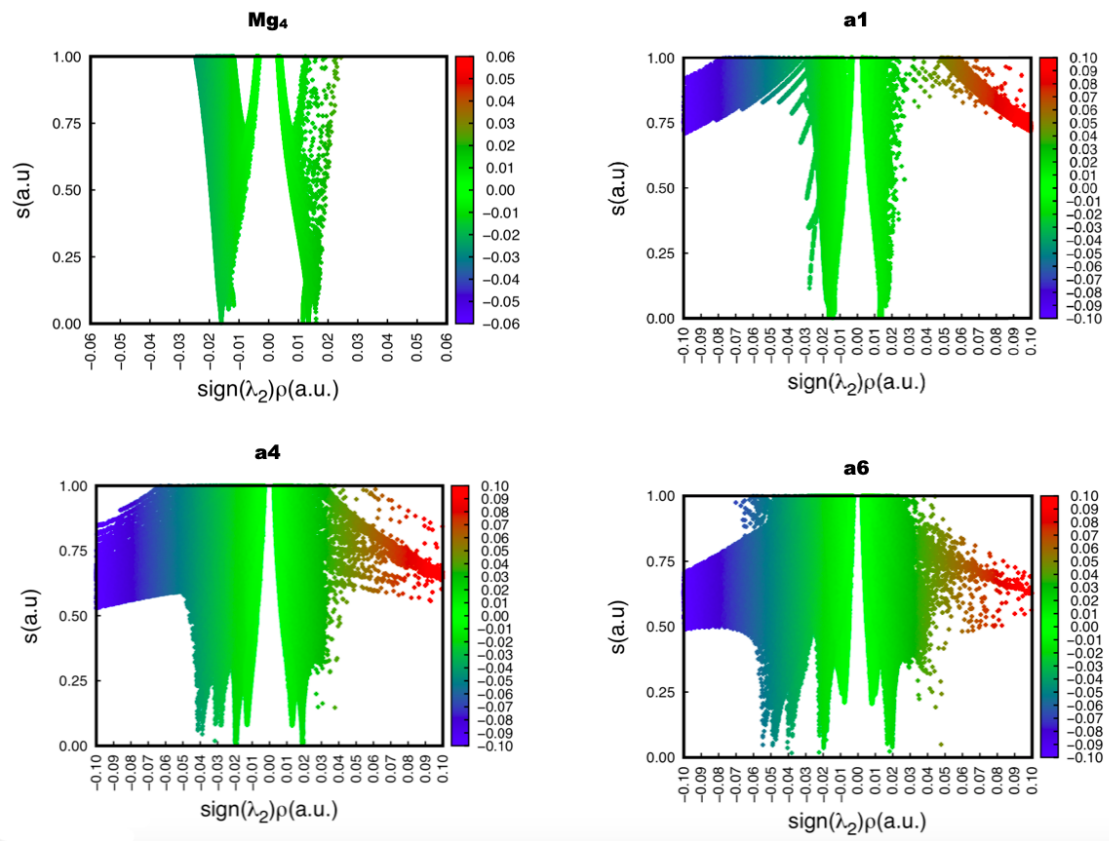


Figure S8. CASSCF orbitals with their occupation numbers included in the (6,6) active space of the isolated HF molecule.



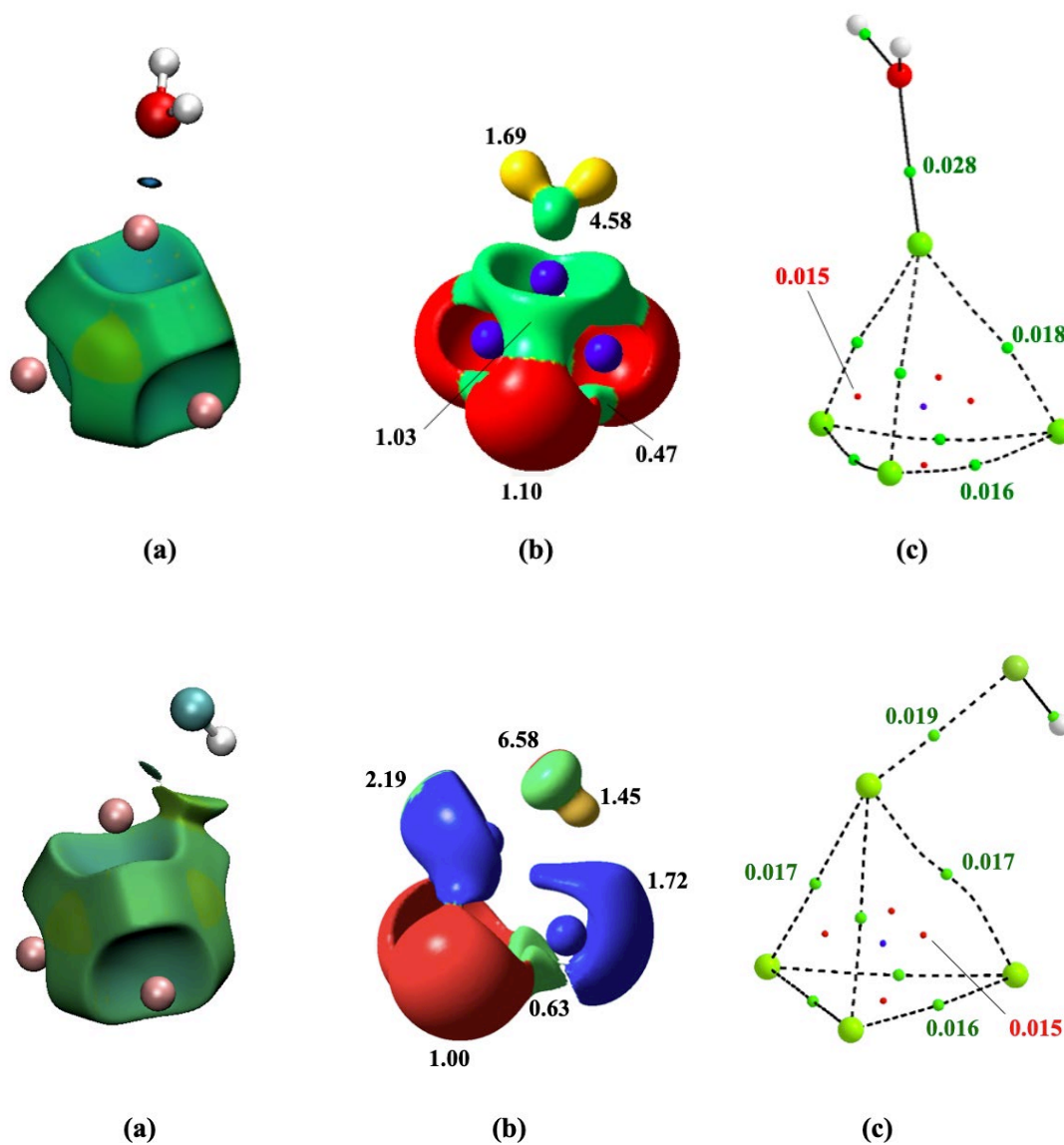


Figure S10. Bonding analysis for $\text{Mg}_4\text{-H}_2\text{O}$ (w1, upper panel) and $\text{Mg}_4\text{-HF}$ (hf1, lower panel) adducts, including the NCI 3D (a), ELF (b) and AIM (c) molecular graphs. (figura temporal!)

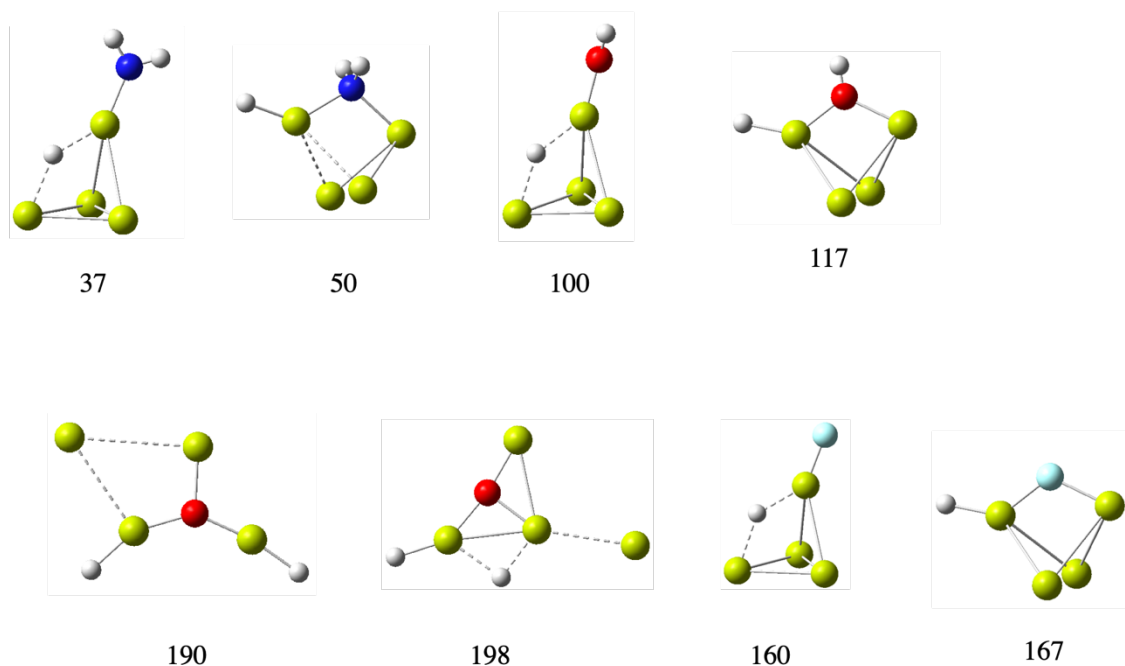


Figure S11. Additional local minima related to the interaction of Mg_4 clusters with ammonia, water and hydrogen fluoride. The G4 binding energies in $\text{kJ}\cdot\text{mol}^{-1}$ are also given.

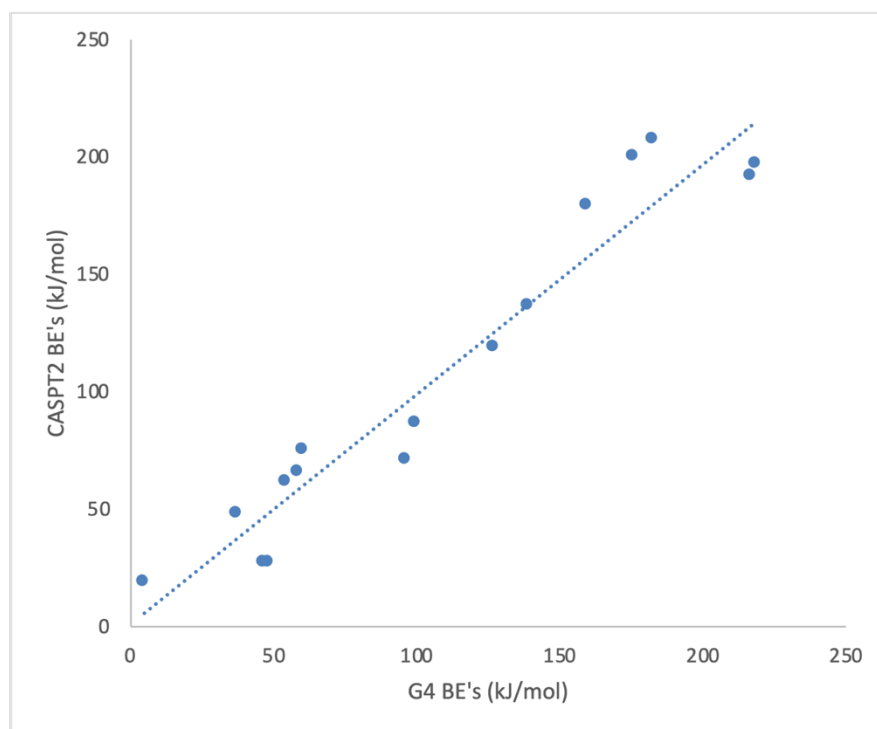


Figure S12. Linear correlation between the CASPT2 and G4 calculated binding energies for complexes of Mg_4 with ammonia, water and hydrogen fluoride. The linear correlation obeys the equation:

$$\text{BE}(\text{CASPT2}, \text{kJ}\cdot\text{mol}^{-1}) = 0.874 \text{ BE}(\text{G4}, \text{kJ}\cdot\text{mol}^{-1}) + 1.223, r^2 = 0.928$$

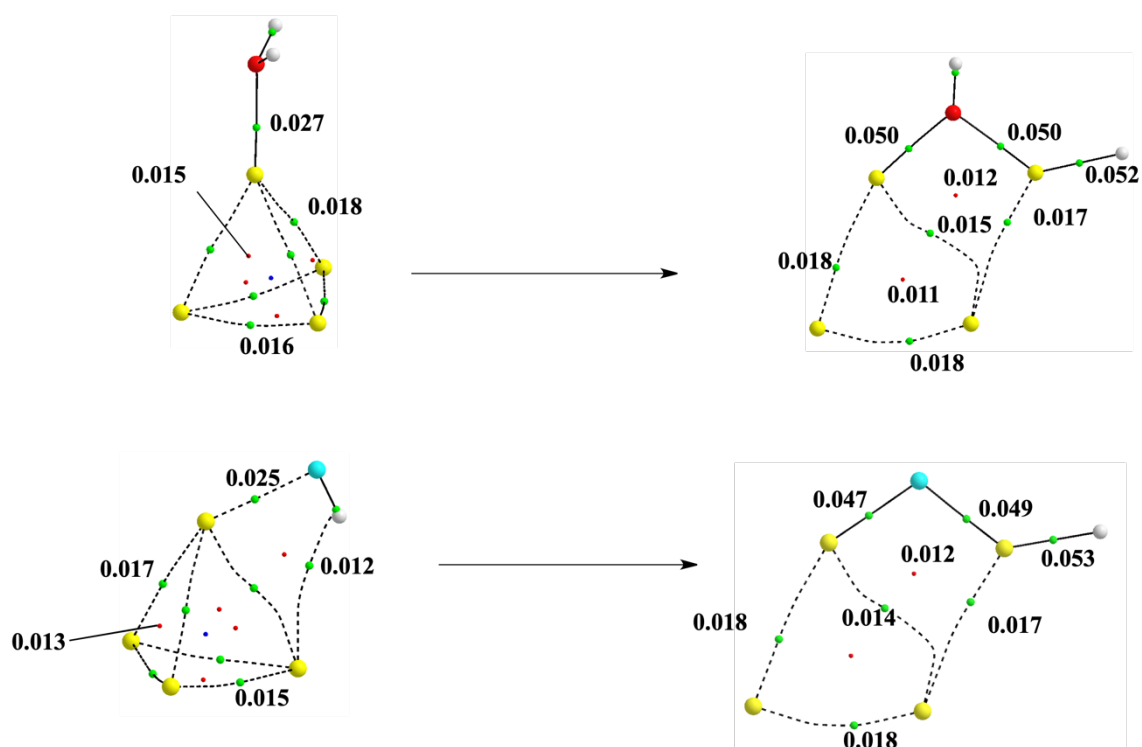


Figure S13. Comparison of the molecular graphs of the adducts of water and hydrogen fluoride to Mg_4 clusters (left column) with those of the most stable local minima in which one of the hydrogens of the base has been transferred towards the Mg_4 moiety (right column). The values of the electron densities at the BCPs clearly show that both X-Mg (X = O, F) bonds in the structures on the right are much higher than the density at these BCPs for the structures on the left, as an evidence of strong Mg-X bond reinforcement in this isomerization process.

Additional computational details for the QTAIM, ELF and NCI calculations.

We have used three topological methods to characterize bonding on the adducts: QTAIM, ELF and NCI. As a complement to what explained in the manuscript, we would like to add here some additional explanations.

The Quantum Theory of Atoms in Molecules (QTAIM) is used to detect covalent and noncovalent interactions through the formation of bond paths between interacting atoms. Critical points are points where the first derivative of the density equals to zero. These points of the space are characterized by their rank (number of non-zero eigenvalues of the Hessian) and their signature (sum of the signs of the eigenvalues). Using rank and signature we distinguish between local maxima (3,-3), bond critical points BCP (3,-1), ring critical points RCP (3,+1), and cage critical points CCP (3,+3). The density and Laplacian of the density is used at the BCP to characterize the strength and nature (covalent/ionic) of the interactions between two given atoms. The molecular graphs in the manuscript show the bond paths along with the BCP, RCP and CCP found for the systems characterized by their electron density.

The ELF (Electron Localization Function) is based on the Pauli repulsion and reveals regions of highly localized electrons such as the core of atoms, lone pairs or bonds, where the Pauli repulsion is low. Basins present a certain amount of electron population and a volume sensible to the chemical environment. These basins may belong to one atom (monosynaptic basins) or several atoms (polysynaptic basins), so they are very useful to provide a Lewis picture of a given system. In 3D representations, basins containing hydrogens appear in yellow color, whereas lone pairs appear in red and bonding regions in green. The ELF is dimensionless and varies between 0 and 1; the higher the ELF value, the larger the electron localization.

Finally, the Non Covalent Interaction (NCI) index is based on the reduced density gradient (RDG). Non-covalent interactions are characterized by both low density and low reduced density gradient values. We can represent these two magnitudes in 2D diagrams

where attractive interactions appear as peaks in the negative part of the x axis and repulsive interactions also appear as peaks in the positive part of the x axis. Using gradient isosurfaces in 3D plots, we can distinguish these same interactions in the real space (blue color for strongly attractive interactions, red color for strongly repulsive interactions, and green for weakly attractive or repulsive interactions). One of the main advantages of NCI is that allows to identify interactions that are blind to the QTAIM analysis.